Solid-liquid equilibria and triple points of *n*-6 Lennard-Jones fluids

Alauddin Ahmed and Richard J. Sadus[a)]
Centre for Molecular Simulation, Swinburne University of Technology, P.O. Box 218, Hawthorn, Victoria 3122, Australia

(Received 5 August 2009; accepted 2 October 2009; published online 2 November 2009)

Molecular dynamics simulations are reported for the solid-liquid coexistence properties of *n*-6 Lennard-Jones fluids, where $n=12$, 11, 10, 9, 8, and 7. The complete phase behavior for these systems has been obtained by combining these data with vapor-liquid simulations. The influence of *n* on the solid-liquid coexistence region is compared using relative density difference and miscibility gap calculations. Analytical expressions for the coexistence pressure, liquid, and solid densities as a function of temperature have been determined, which accurately reproduce the molecular simulation data. The triple point temperature, pressure, and liquid and solid densities are estimated. The triple point temperature and pressure scale with respect to $1/n$, resulting in simple linear relationships that can be used to determine the pressure and temperature for the limiting ∞-6 Lennard-Jones potential. The simulation data are used to obtain parameters for the Raveché, Mountain, and Streett and Lindemann melting rules, which indicate that they are obeyed by the *n*-6 Lennard Jones potentials. In contrast, it is demonstrated that the Hansen–Verlet freezing rule is not valid for *n*-6 Lennard-Jones potentials. © *2009 American Institute of Physics*.
[doi:10.1063/1.3253686]

I. INTRODUCTION

Intermolecular interactions involved in solid-liquid coexistence are of considerable scientific interest.[1] Theories of solid-liquid coexistence are commonly based on the observation that the structure of dense fluids is dominated by steep repulsive interaction between the atoms or molecules.[2–5] Melting temperatures are strongly influenced by interatomic repulsive forces. The 12-6 Lennard-Jones potential is adequate for atomic fluids, whereas modeling the behavior of molecules or monomers of polymer chains usually requires a potential with a softer repulsive part.[6]

A simple soft core potential can be obtained by replacing the "12" exponent in the 12-6 Lennard-Jones potential by a smaller integer. It has been found that varying the value of this exponent and, thereby the steepness of the main repulsive branch of the potential, significantly affects vapor-liquid equilibria,[6–9] the critical point,[7] and transport properties.[10–12] Although a number of molecular simulation studies[6–9] of vapor-liquid equilibria have been reported for such *n*-6 Lennard-Jones potentials, the effect of varying *n* for the solid-liquid phase transition has not been widely investigated. The absence of solid-liquid equilibrium data can be partly attributed to the difficulty of particle insertion between dense phases common to many molecular simulation techniques. This difficulty has been recently eliminated by a molecular dynamics (MD) algorithm[13] that combines aspects of equilibrium and nonequilibrium simulation techniques.

In this work, we use the combined[13] equilibrium molecular dynamics (EMD) and nonequilibrium molecular dynamics (NEMD) approach to investigate solid-liquid coexistence of *n*-6 Lennard-Jones fluids as a function of *n*. The data provide an insight into the role of intermolecular repulsion on the solid-liquid transition. We demonstrate how physical properties and the melting rules vary with *n*. The data also allow us to complete the phase diagrams of the *n*-6 Lennard-Jones fluids and estimate the triple points.

II. SIMULATION DETAILS

The *n*-6 Lennard-Jones potential is

$$u(r) = \varepsilon\left(\frac{n}{n\text{-}6}\right)\left(\frac{n}{6}\right)^{\frac{6}{n\text{-}6}}\left[\left(\frac{\sigma}{r}\right)^{n} - \left(\frac{\sigma}{r}\right)^{6}\right], \quad (1)$$

where σ is the atomic diameter and ε is the well depth. We will consider potentials with values of *n* ranging from 7 to 12. The smaller the index *n*, the wider the attractive part and

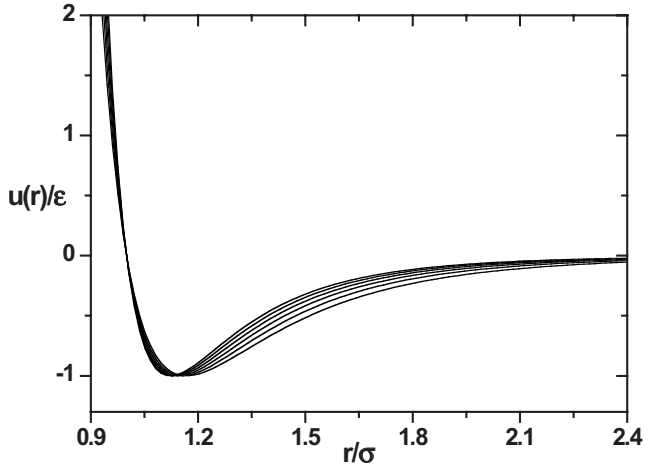

FIG. 1. Comparison of *n*-6 Lennard-Jones pair potentials where from top to bottom $n=12$, 11, 10, 9, 8, and 7.

[a)]Electronic mail: rsadus@swin.edu.au.

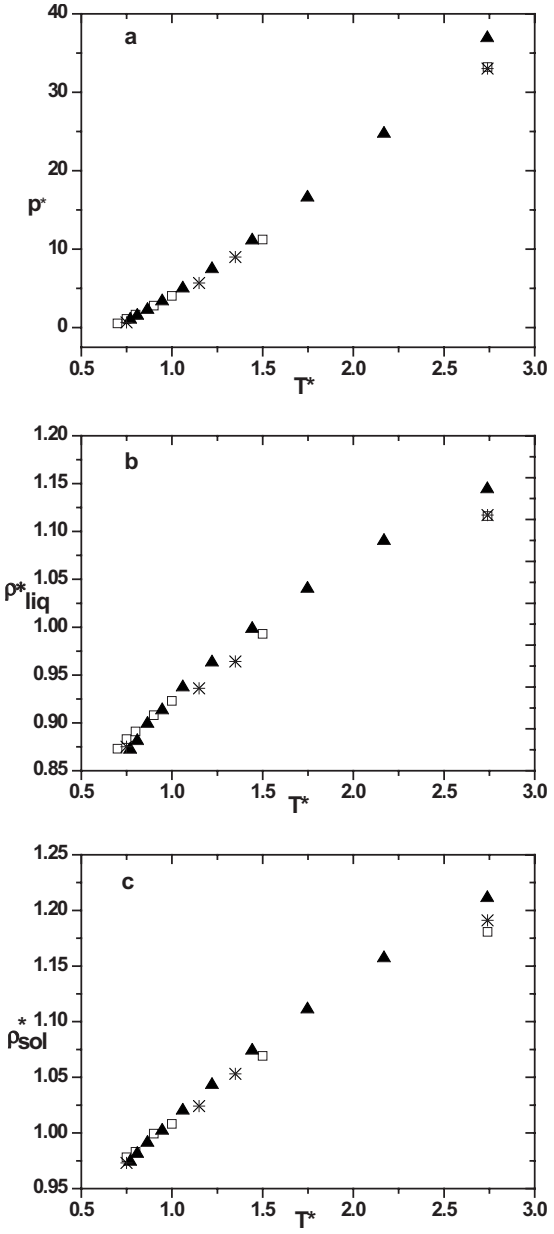

FIG. 2. Comparison of the solid-liquid coexistence (a) pressure, (b) liquid densities, and (c) solid densities for the 12-6 Lennard-Jones potential calculated in this work (□) with data from the literature (▲ Ref. 15, * Ref. 16). The errors are approximately equal to the symbol size.

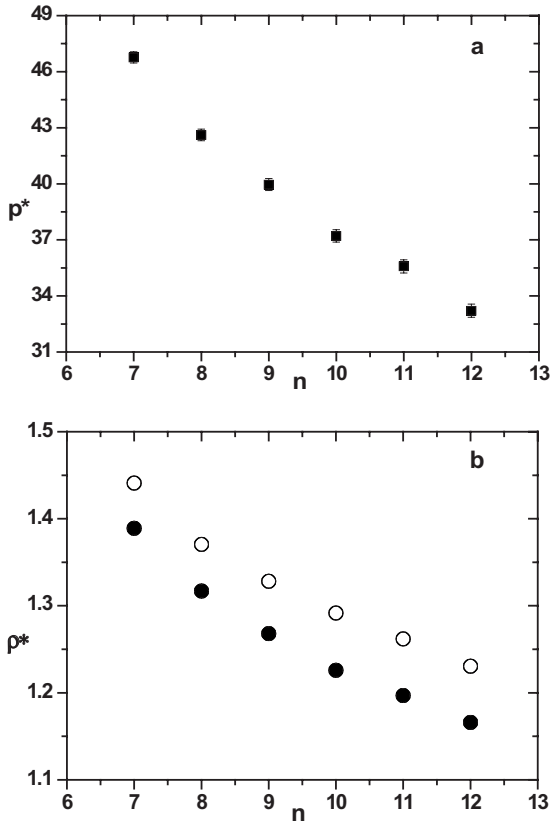

FIG. 3. Comparison of the solid-liquid coexistence (a) pressure (■) and (b) liquid (●) and solid (o) densities of n-6 Lennard-Jones potentials at $T=2.74$.

weaker the repulsive force, as depicted in Fig. 1. It should be noted that attributing n and "6" contributions to repulsion and attraction, respectively, is only a convenient approximation. The continuous nature of the potential with respect to interatomic separation (r) means that it is impossible to isolate either purely repulsive or purely attractive contributions. As n approaches infinity, the leading coefficient of Eq. (1) approaches ε and the n-6 Lennard-Jones potential reaches the limiting case of a "hard-sphere+attractive term" potential.[8]

We have used the simulation algorithm proposed by Ge *et al.*[13] that combines the techniques of both EMD and NEMD. We denote this algorithm as "GWTS" after the authors. As discussed elsewhere,[13,14] the GWTS algorithm uses NEMD to determine the pressure at different strain rates for a common temperature and density. At densities equal to or greater than the freezing point, there is an abrupt change in pressure between the zero strain-rate case and the first nonzero strain rate, which allows us to accurately identify the freezing density and pressure. Having identified the freezing point, EMD calculations are performed to obtain the isothermal pressure-density behavior of the solid curve. The density of the melting point is the point at which the constant pressure tie line touches the solid curve. In contrast to other methods,[15–25] the GWTS algorithm is self-starting and it does not require particle interchange between phases.

The initial configuration in all the simulations was a face centered cubic lattice structure. The isothermal isochoric NEMD simulations were performed by applying the standard *sllod* equations[26] of motion for planer Couette flow coupled with Lees–Edwards[13,26] periodic boundary conditions. If the applied strain rate is switched off, the *sllod* algorithm behaves like a conventional equilibrium dynamics algorithm in the canonical ensemble (NVT). The NVT EMD simulations were performed using conventional cubic periodic boundary conditions.[27] A Gaussian thermostat multiplier[28] was used to keep the kinetic temperature of the fluid constant. The equations of motion were integrated with a five-value Gear predictor corrector scheme.[27,29] The normal convention was used for the reduced density ($\rho^*=\rho\sigma^3$), temperature ($T^*=kT/\varepsilon$), energy ($E^*=E/\varepsilon$), pressure ($p^*=p\sigma^3/\varepsilon$), and time ($\tau^*=[\varepsilon/m\sigma^2]^{1/2}\tau$). All quantities quoted in this work are in terms of these reduced quantities and the asterisk superscript will be omitted in the rest of the paper.

TABLE I. Molecular simulation data for the solid-liquid coexistence properties of n-6 Lennard-Jones fluids. The statistical uncertainties are given in parenthesis.

T^*	n	p^*	ρ^*_{liq}	E^*_{liq}	ρ^*_{sol}	E^*_{sol}	Δh^*
2.74	7	46.7(3)	1.339	−4.72(7)	1.391	−5.83(7)	−2.41
	8	42.6(3)	1.267	−4.01(7)	1.321	−5.14(7)	−2.48
	9	39.9(3)	1.218	−3.66(6)	1.278	−4.73(7)	−2.61
	10	37.2(3)	1.176	−3.53(6)	1.242	−4.60(7)	−2.73
	11	35.5(3)	1.147	−3.45(6)	1.212	−4.55(7)	−2.76
	12	33.2(3)	1.116	−3.48(6)	1.181	−4.60(6)	−2.75
1.5	7	12.8(1)	1.111	−8.44(3)	1.170	−9.33(3)	−1.47
	8	12.7(1)	1.074	−7.35(4)	1.138	−8.19(3)	−1.51
	9	11.9(1)	1.039	−6.64(3)	1.102	−7.64(3)	−1.65
	10	11.7(1)	1.021	−6.19(3)	1.090	−7.09(3)	−1.63
	11	11.7(1)	1.009	−5.87(3)	1.078	−6.79(3)	−1.66
	12	11.2(1)	0.993	−5.63(3)	1.069	−6.57(3)	−1.74
1.0	7	3.22(9)	0.989	−9.13(2)	1.052	−10.01(2)	−1.06
	8	3.77(9)	0.967	−7.99(2)	1.035	−8.86(2)	−1.12
	9	3.89(9)	0.948	−7.26(2)	1.024	−8.15(2)	−1.19
	10	3.9(1)	0.935	−6.77(2)	1.014	−7.67(2)	−1.23
	11	4.0(1)	0.929	−6.41(2)	1.008	−7.33(2)	−1.25
	12	4.05(1)	0.923	−6.14(2)	1.008	−7.05(2)	−1.28
0.90	7	1.63(7)	0.965	−9.18(2)	1.031	−10.08(2)	−1.01
	8	2.17(7)	0.939	−8.04(2)	1.012	−8.93(2)	−1.05
	9	2.40(8)	0.924	−7.31(2)	1.003	−8.22(2)	−1.11
	10	2.63(9)	0.917	−6.83(2)	1	−7.76(2)	−1.16
	11	2.80(9)	0.913	−6.48(2)	1	−7.43(2)	−1.21
	12	2.7(1)	0.908	−6.21(1)	0.999	−7.18(2)	−1.24
0.80	7	0.39(6)	0.937	−9.22(1)	1.012	−10.15(2)	−0.96
	8	0.82(6)	0.913	−8.07(1)	0.992	−8.99(20	−0.99
	9	1.10(7)	0.9	−7.34(1)	0.990	−8.31(2)	−1.07
	10	1.41(7)	0.898	−6.88(1)	0.984	−7.83(1)	−1.08
	11	1.43(8)	0.892	−6.53(1)	0.983	−7.49(2)	−1.10
	12	1.65(8)	0.891	−6.25(1)	0.983	−7.23(1)	−1.15

The results presented here are the ensemble averages for five independent simulations corresponding to different MD trajectories. The simulation trajectories were typically run for 2×10^5 time steps of $\tau=0.001$. The first 5×10^4 time steps of each trajectory were used either to equilibrate zero-shearing field EMD or to achieve nonequilibrium steady state after the shearing field was switched on. The rest of the time steps in each trajectory were used to accumulate the average values of thermodynamic variables and standard deviations. A system size of 2048 Lennard-Jones particles was used for all the simulations with a cutoff distance of 2.5σ. Conventional long-range corrections were used to recover the properties of the full Lennard-Jones fluid.

III. RESULTS AND DISCUSSION

A. Solid-liquid coexistence

To validate the GWTS simulation method[13] we first calculated solid-liquid equilibria for the 12-6 Lennard-Jones system at various temperatures and compared the results with data available in the literature (Fig. 2).[15,16] Figure 2 shows that our results for the pressure-temperature behavior are in good agreement with previous studies. The only exception is that the pressure at $T=2.74$ is somewhat lower than reported elsewhere.[15] This discrepancy in pressure reflects the fact that our results for both freezing and melting points occur at different densities [Figs. 2(b) and 2(c)]. Our densities are lower than reported by Agrawal and Kofke.[15] Agrawal and Kofke's pressure data are 12% higher then the data of Hansen and Verlet.[16] The cause of this discrepancy is commonly attributed to uncertainties in the starting point required by the Gibbs–Duhem integration (GDI) method.[24,25] The inverse 12th-power soft-sphere initial condition needed to start the GDI procedure was $p=16.89T^{5/4}$, which is higher than reported by Hoover *et al.*,[30] Hansen,[16] and Cape and Woodcock.[31] Any error in the initial condition for the GDI method will be systematically[32] applied to all other state points. The GWTS algorithm[13] used in this work is free from this uncertainty.

The solid-liquid coexistence pressure as a function of n is shown in Fig. 3(a) for $T=2.74$. It indicates that there is an approximately linear inverse relationship between pressure and n. Decreasing the value of n causes an increase in the coexistence pressure. Decreasing the value of n means the distance at which atoms start to experience significant repulsive forces is decreased. Therefore, higher pressures are required to overcome this increased repulsion to form a solid phase. The coexisting solid and liquid densities for different n values are illustrated in Fig. 3(b). In common with the coexistence pressure, decreasing the value of n causes both the liquid and solid phase coexisting densities to increase.

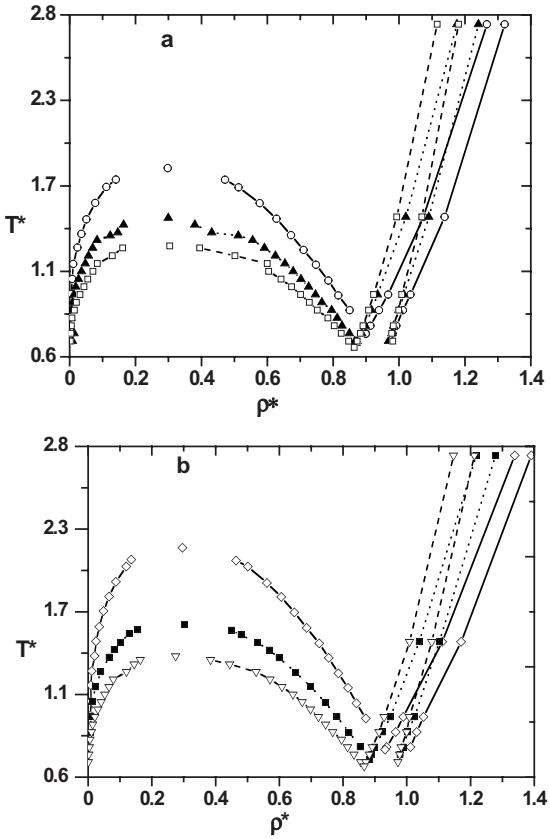

FIG. 4. Complete density-temperature phase diagrams of n-6 Lennard-Jones potentials. Shown are (a) $n=12$ (□, guided by a dashed line), 10 (▲, guided by a dotted line), 8 (O, guided by a solid line) and (b) $n=7$ (◇, guided by a solid line), 9 (■, guided by a dotted line), 11 (△, guided by a dashed line). The vapor-liquid coexistence data are from Refs. 7 and 9. Freezing and melting lines and triple points are from this work.

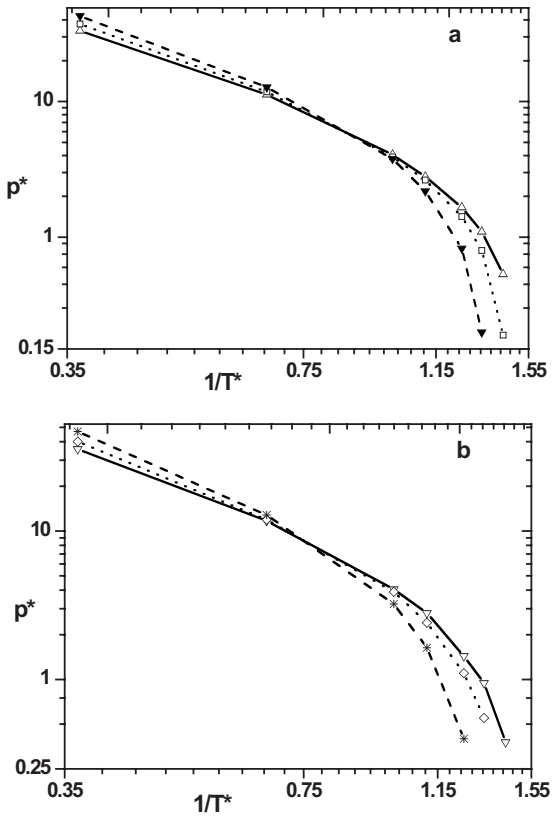

FIG. 5. The solid-liquid coexistence pressure of n-6 Lennard-Jones potentials calculated in this work as a function of reciprocal temperature on a log scale. (a) $n=12$ (△, guided by a solid line), 10 (□, guided by a dotted line), and 8 (▼, guided by a dashed line). (b) $n=11$ (▽, guided by a solid line), 9 (◇, guided by a dotted line), and 7 (*, guided by a dashed line).

However, the relationship is not linear and the difference between the liquid and solid densities decreases slightly with decreasing n. These data and data for other temperatures are summarized in Table I. The data for the other temperatures show the same trend as $T=2.74$. The energy and change in enthalpy are also given in Table I for the benefit of completeness.

The temperature-density behavior of the freezing and melting lines of n-6 Lennard-Jones potentials is illustrated in Fig. 4. Vapor-liquid coexistence data[7,9] and triple point data are also included to complete the phase diagram of the pure n-6 Lennard-Jones fluids. Figure 4(a) represents the complete phase diagrams for $n=12$, 10, and 8 and Fig. 4(b) represents the complete phase diagrams for $n=11$, 9, and 7. It is well known[7,9] that a decrease in the value of n increases the temperature of the critical point, increasing the temperature range for two-phase vapor-liquid coexistence. The main effect of decreasing n on solid-liquid coexistence is to shift the melting and freezing curves to higher densities.

The variation in pressure for different n values with respect to temperature is examined in Figs. 5(a) and 5(b). At high temperatures, the pressure decreases with increasing n. However, this trend is reversed at medium to low temperatures, at which pressure increases with increasing n. The most notable change occurs at very low temperatures, where an increase in the value of n results in a sharp increase in pressure.

The solid-liquid coexistence region of the phase diagram is sensitive to the nature of the interaction potential.[33] The relative density difference (rdd) and the fractional density change (fdc) at freezing (commonly known as the miscibility gap) are two measures that can be used to quantify the effect of the interaction potential on solid-liquid coexistence. The rdd is defined as[34] $\delta n=2(\rho_{sol}-\rho_{liq})/(\rho_{sol}+\rho_{liq})$, where ρ_{sol} and ρ_{liq} are the solid and liquid coexistence densities of the system. The lower bound of the rdd is 0.037, which is the approximate value for 12-inverse-power soft sphere systems.[35] The upper bound is 0.098, which is the rdd for hard spheres.[36] The n dependency of the rdd is shown in Fig. 6(a). We have also calculated the rdd of the 12-6 Lennard-Jones system from Agrawal and Kofke's[15] data, obtaining a value of 0.093. The miscibility gap or fdc is defined as[15,33] $(\rho_{sol}-\rho_{liq})/\rho_{liq}$ and is shown in Fig. 6(b). It is evident that both fdc and rdd decrease with decreasing n values. This means that decreasing n results in a smaller two-phase region. Both metrics also decrease significantly with the increasing temperature. Therefore, the size of the two-phase region is narrower at high temperatures compared with low temperatures.

B. Temperature dependence of coexistence pressure and densities

At high temperatures repulsive force dominates and it is expected that the 12-6 Lennard-Jones potential must ap-

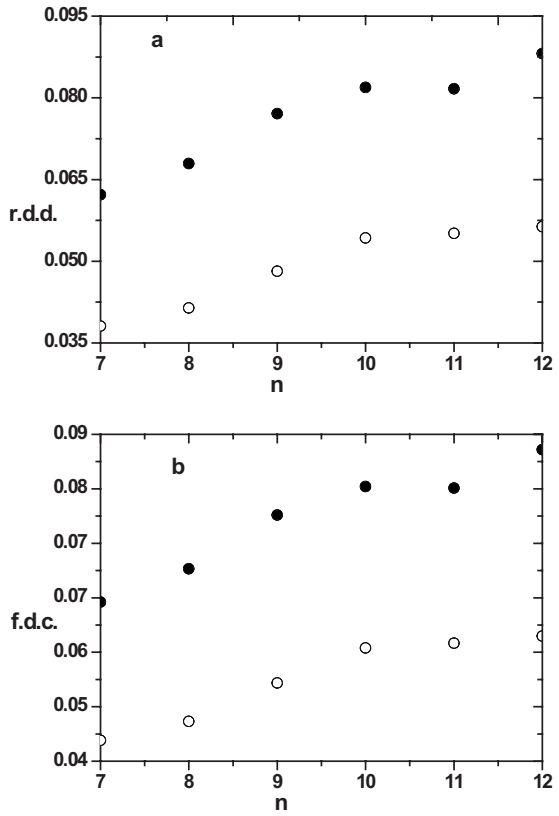

FIG. 6. (a) rdd and (b) fdc of n-6 Lennard-Jones potentials at $T=1.0$ (●) and $T=2.74$ (○).

proach the scaling behavior of the inverse 12th-power potential.[35] Using the special scaling properties[35,37,38] of the inverse nth-power potential, Agrawal and Kofke[15] showed that

$$p_{12\text{-}6} = \beta^{-5/4} \exp(-D\beta^{1/2})[16.89 + k_1\beta + k_2\beta^2], \quad (2)$$

where $\beta=1/kT$, 16.89 is the limiting soft sphere value of $p\beta^{5/4}$, $D=0.4759$ was determined from soft-sphere simulation data, and k_1 and k_2 are fitting parameters. van der Hoef[39] used Eq. (2) to reproduce the solid-liquid coexistence data with very good accuracy. For soft-core systems, the equilibrium melting temperature and pressure should satisfy $C_n = p\beta^{\alpha}$, where $\alpha=(3+n)/n$. Morris *et al.*[22] reported values of $C_{12}=16.89\pm0.03$ and $C_9=22.90\pm0.03$ for soft sphere potentials. We propose that Agrawal and Kofke's[15] original semiempirical fit can be generalized for any n-6 Lennard-Jones potential,

$$p_{n\text{-}6} = \beta^{-(3+n)/n} \exp(-0.4759\beta^{1/2})[k_0 C_{12} + k_1\beta + k_2\beta^2]. \quad (3)$$

The values of k_0, k_1, and k_3 obtained from fitting our simulation data to Eq. (3) are summarized in Table II. Equation (3) accurately reproduces the pressure-temperature behavior ($0.8 \le T \le 2.74$) as evident from a squared correlation coefficient (R^2) value of 0.99 for all n-6 Lennard-Jones potentials.

van der Hoef[39] fitted the freezing and melting densities for a 12-6 Lennard-Jones via the following relationships involving β:

TABLE II. Parameters for the scaling behavior [Eq. (3)] of pressure as a function of inverse temperature for n-6 Lennard-Jones potentials. Errors are given in parenthesis.

n	k_0	k_1	k_2
12	1.36(1)	−20.5(6)	3.8(4)
11	1.49(1)	−23.6(9)	4.7(5)
10	1.61(2)	−27(1)	6.3(8)
9	1.82(4)	−34(2)	9(1)
8	1.93(2)	−35(1)	8(1)
7	2.28(3)	−48(2)	15(1)

$$\left.\begin{aligned} \rho_{\text{liq}} &= \beta^{-1/4}[l_0 + l_1\beta + l_2\beta^2 + l_3\beta^3 + l_4\beta^4 + l_5\beta^5] \\ \rho_{\text{solid}} &= \beta^{-1/4}[s_0 + s_1\beta + s_2\beta^2 + s_3\beta^3 + s_4\beta^4 + s_5\beta^5] \end{aligned}\right\}. \quad (4)$$

We found that simulation data for all of the n-6 Lennard-Jones potentials could be accurately ($R^2=0.99$) fitted to these equations. The values of the required parameters are summarized in Table III.

C. Estimation of the triple point

We have obtained estimates of the triple point by performing solid-liquid equilibria simulations at low densities and, where necessary, slightly extrapolating vapor-liquid data. The triple point liquid density and temperature were identified by the intersection of the solid-liquid and vapor-liquid coexistence data. The solid densities were estimated by extrapolating data for the melting densities to the triple point temperature. We have determined the triple point pressures from extrapolating our solid-liquid coexistence data for $T<0.8$. The use of extrapolation means that the triple point values should only be considered as good approximations rather than accurate values.

Triple point data in the literature are confined exclusively to the 12-6 Lennard-Jones potential. The estimated triple point for the 12-6 Lennard-Jones potential is compared with literature sources in Table IV. Our triple point temperature differs by less than 4% from the values reported by either Hansen and Verlet[16] or Agrawal and Kofke.[15] Indeed, it is well within the uncertainty reported by Hansen and Verlet.[16] Our triple point densities are somewhat higher than reported earlier.[15,16] The triple point pressure is higher than reported elsewhere,[15] reflecting differences in both the estimated triple point temperature and densities. We note that estimating the pressure is prone to considerable uncertainties[40] with early estimates yielding negative values.[18] The differences between our calculations and that of Agrawal and Kofke can be partly attributed to the effect of system size. Agrawal and Kofke observed a 1.6% decrease in temperature by increasing the system size from 236 to 932 atoms. In contrast, 2048 atoms were used for our simulations in the vicinity of the triple point.

The triple points for the remaining n-6 Lennard-Jones potentials are summarized in Table V. We were not able to reliably determine the pressures for $n=7$ and 8 because of the precipitous nature of the pressure change close to the triple point. For other n values a scaling relationship for both

TABLE III. Parameters for the polynomial fit [Eq. (4)] for the coexisting liquid and solid densities for n-6 Lennard-Jones potential.

n	l_0	l_1	l_2	l_3	l_4	l_5	s_0	s_1	s_2	s_3	s_4	s_5
12	1.439 85	1.319 19	1.586 85	1.827 55	1.687 77	1.860 46	0.636 19	4.494 82	−12.9164	15.895 34	−9.073 14	1.971 57
11	−1.3116	−0.190 95	−1.682 11	−2.666 71	−1.5078	−1.892 77	0.882 57	3.1642	−9.784 99	12.137 58	−6.849 99	1.459 31
10	1.484 22	−1.498 35	1.986 72	3.477 35	1.078 35	1.414 98	1.973 16	−3.807 65	7.138 75	−7.304 66	3.798 66	−0.783 07
9	−1.016 81	2.526 47	−1.496 15	−2.250 97	−0.293 79	−0.393 37	1.849 97	−2.434 89	2.9722	−1.779 39	0.414 64	0
8	0.395 61	−1.579 08	0.680 41	0.560 61	0	0	1.744 61	−1.587 36	1.371 56	−0.603	0.108 72	0
7	−0.068 12	0.352 03	−0.140 72	0	0	0	1.874 03	−1.720 06	1.1946	−0.296 28	0	0

triple point temperature [Fig. 7(a)] and pressure [Fig. 7(b)] with respect to $1/n$ can be observed. In contrast, scaling behavior is not apparent for the densities [Fig. 7(c)]. These data can be adequately fitted by

$$\left.\begin{aligned} T_{\mathrm{tr}}(n) &= 2.10/n + 0.482 \\ p_{\mathrm{tr}}(n) &= 0.1104/n - 0.0073 \end{aligned}\right\}. \tag{5}$$

From Eq. (5), the triple point temperature for the ∞-6 Lennard-Jones potential is 0.482. The relatively small value of the intercept for the pressure equation suggests that the triple point pressure for the ∞-6 Lennard-Jones potential is zero. This compares with a critical temperature of either 0.572 or 0.607 reported by Camp and Patey[41] and Charpentier and Jakse,[8] respectively, and a critical pressure[41] of 0.079. These data are likely to be of value in calibrating hard sphere+attractive term equations of state.[42]

D. Melting and freezing rules

It has been observed that liquid freezing and solid melting follow certain empirical rules. Most freezing rules involve the liquid structure as quantified by the radial distribution function, whereas melting rules typically involve either geometrical attributes or free energy calculations. In view of this, it is of interest to examine the radial distribution function for the n-6 Lennard-Jones fluids. Figure 8 compares the radial distribution functions for the 12-6 Lennard-Jones and 7-6 Lennard-Jones potentials at a common state point. It is apparent that decreasing the value of n results in higher maxima and lower minima, resulting in narrower peaks. Figure 9 compares the radial distribution maxima [Fig. 9(a)] and minima [Fig. 9(b)] for different n-6 Lennard-Jones fluids at the freezing point. It is evident that the choice of n has a considerable influence of the structure of the fluid at the freezing transition.

The Lindemann,[43] Simon–Glatzel,[44,45] and Ross[46] rules are widely used examples of melting rules. The most commonly used freezing rules are the Hansen–Verlet,[16] Raveché–Mountain–Streett (RMS),[17] and Giaquinta–Giunta[47] rules. Agrawal and Kofke[15] concluded that many melting and freezing rules were both temperature and density dependent. In contrast, the freezing rule of RMS is almost invariant for the entire solid-liquid coexistence curve from the triple point to the high temperature soft-sphere limit.

RMS observed[17] that experimental radial distribution function data generally obeyed the following relationship:

$$I_{\mathrm{RMS}} = g(r_{\mathrm{min}})/g(r_{\mathrm{max}}) \approx 0.2, \tag{6}$$

where r_{min} is the position of the first nonzero minimum of the pair distribution and r_{max} is the position of its first maximum. We calculated I_{RMS} from our simulation data for the n-6 Lennard-Jones potentials at a common temperature of $T=1.0$ (Table VI). It is apparent from Table VI that I_{RMS} is largely invariant for all values of n. The difference in the value of I_{RMS} (0.14) for the 12-6 Lennard-Jones potential compared with the experimentally observed value (0.2) partly reflects the limitation of the potential to fully represent the properties of real fluids.

The Hansen–Verlet[16] rule states that on freezing the structure factor has a maximum value of $S(k_0)=2.85$. We have obtained the structure factor[4] via a Fourier transformation of the pair-correlation function. Hansen[16] found that $S(k)$ changes with increasing temperature for 864 particles. Agrawal and Kofke[15] also observed a 10% variation in this value with respect to temperature change. They also found that the Hansen–Verlet freezing rule also varied significantly with system size. For a system of 2048 12-6 Lennard-Jones atoms at $T=2.74$ we calculated the maximum structure factor to be 4.2. Values for other n-6 Lennard-Jones potentials are summarized in Table VI. It is evident from the data in Table

TABLE IV. Comparison of triple point properties for the 12-6 Lennard-Jones fluid obtained from molecular simulation studies. Errors are given in parenthesis.

Source	System size	T^*_{tr}	p^*_{tr}	$\rho^*_{\mathrm{liq,tr}}$	$\rho^*_{\mathrm{sol,tr}}$
Ladd and Woodcock[a]	1500	0.67(1)	−0.47(3)	0.818(4)	0.963(6)
Hansen and Verlet[b]	864	0.68(2)	⋯	0.85(1)	⋯
Agrawal and Kofke[c]	236	0.698	0.0013	0.854	0.963
Agrawal and Kofke[c]	932	0.687(4)	0.0011	0.850	0.960
This work	2048	0.661	0.0018	0.864	0.978

[a]Reference 18.
[b]Reference 16.
[c]Reference 15.

TABLE V. Estimated triple point properties for n-6 Lennard-Jones potentials.

n	T^*_{tr}	p^*_{tr}	$\rho^*_{liq,tr}$	$\rho^*_{sol,tr}$
∞	0.482	0	⋯	⋯
12	0.661	0.0018	0.864	0.978
11	0.673	0.0028	0.867	0.982
10	0.689	0.0038	0.867	0.992
9	0.718	0.0049	0.883	1.000
8	0.748	⋯	0.899	1.028
7	0.782	⋯	0.932	1.050

VI that the value of $S(k_0)$ depends on the value of n. This means that the Hansen–Verlet freezing rule is not valid for n-6 Lennard-Jones potentials.

The most commonly used model for predicting the melting line is the Lindemann rule.[43] The Lindemann ratio (L) is

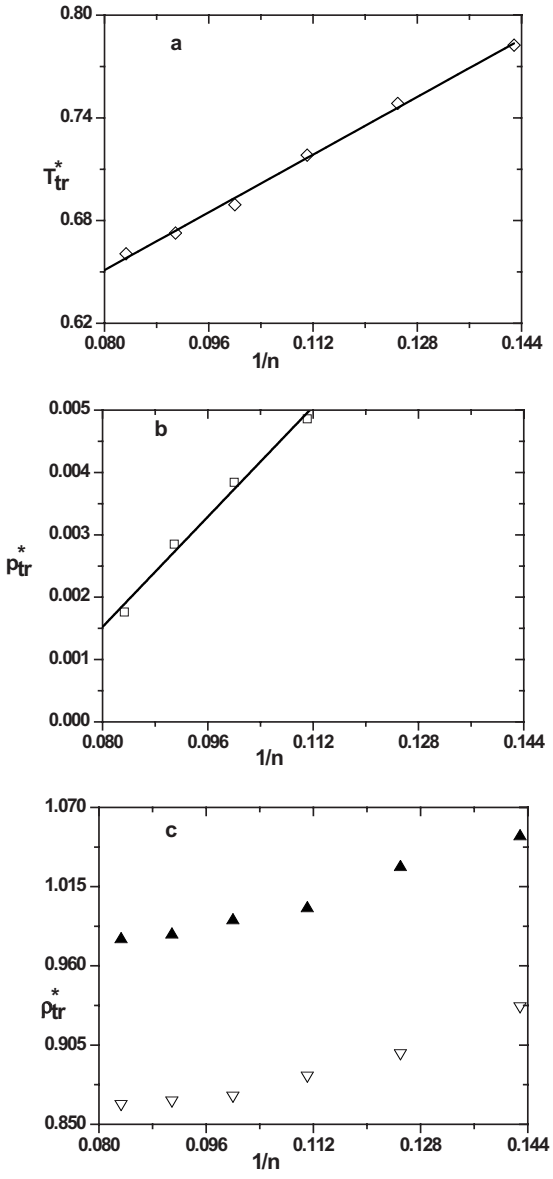

FIG. 7. Triple point properties of n-6 Lennard-Jones potentials as a function of $1/n$. Shown are (a) triple point temperatures (◇), (b) pressures (□), and (c) liquid (▽) and solid (▲) phase densities. The lines represent the least-squares fit of the data given by Eq. (5).

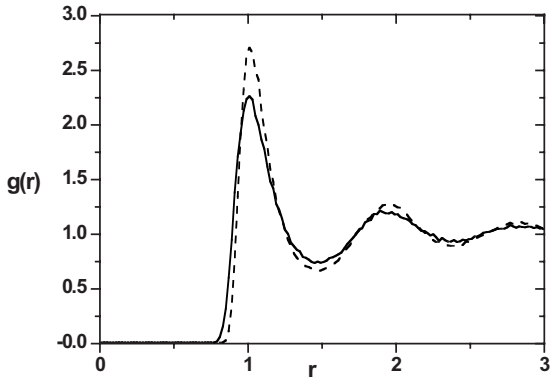

FIG. 8. Comparison of the liquid phase radial distribution functions for a 12-6 Lennard-Jones potential (solid line) and a 7-6 Lennard-Jones potential (dashed line) at $T=2.74$ and $\rho=1.0$.

defined as the root-mean-square displacement of particles in a crystalline solid about their equilibrium lattice positions divided by the nearest neighbor distance (a). In a MD simulation, L can be evaluated[48] via

$$L = \frac{\sqrt{\langle \langle r_i^2 \rangle_t - \langle r_i \rangle_t^2 \rangle_i}}{a}, \tag{7}$$

where $\langle \cdots \rangle_t$ and $\langle \cdots \rangle_i$ denote ensemble averages over time and particles. The Lindemann rule states that a solid melts if the root-mean-square displacement of particles around their ideal position is approximately 10% of their nearest neighbor distance, i.e., $L \approx 0.1$. Many authors[15,16,48] have questioned

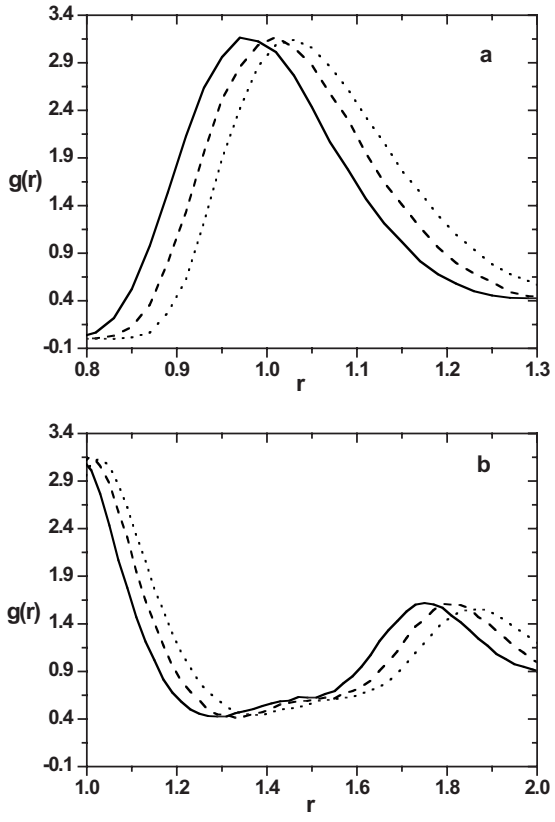

FIG. 9. Comparison of the (a) first maxima and the (b) first minima at the freezing point for n-6 Lennard-Jones fluids, where $n=7$ (solid line), 9 (dashed line), and 12 (dotted line). $T=2.74$ and $\rho=1.339$, 1.218, and 1.116 for $n=7$, 9, and 12, respectively.

TABLE VI. Summary of parameters for melting and freezing rules for n-6 Lennard-Jones potentials at $T=1.0$.

n	$I_{\mathrm{RMS}}=\frac{g(r_{\mathrm{min}})}{g(r_{\mathrm{max}})}=\mathrm{const}$	Lindemann ratio	Maximum in $S(k_0)$
12	0.14	0.157	4.4
11	0.14	0.186	4.8
10	0.13	0.186	5.28
9	0.13	0.181	5.87
8	0.13	0.182	6.57
7	0.13	0.181	7.52

the quantitative prediction of Lindemann's rule, although it is generally accepted as being at least qualitatively correct. We have calculated the Lindemann ratio for all n-6 Lennard-Jones potentials (Table VI) and as expected, $L\neq 0.1$. Nonetheless, L is close to being constant irrespective of the value of n, which indicates that it is a valid indicator of the melting transition.

IV. CONCLUSIONS

The GWTS algorithm[13] is effective in determining solid-liquid equilibrium without relying on either particle insertion or starting values. We have determined the solid-liquid coexistence properties of fluids from the triple point to high pressures, interacting via n-6 Lennard-Jones potentials, where $n=12$, 11, 10, 9, 8, and 7. By combining these data with early vapor-liquid simulation, the complete phase behavior for these systems has been obtained. Analytical expressions for the coexistence pressure liquid and solid densities as a function of temperature have been determined, which accurately reproduce the molecular simulation data. The triple point temperature, pressure, and liquid and solid densities have been estimated. The triple point temperature and pressure scale with respect to $1/n$, resulting in simple linear relationships that can be used to determine the pressure and temperature for the limiting ∞-6 Lennard-Jones potential. Data are obtained for the RMS and Lindemann melting rules, which indicate that they are obeyed by the n-6 Lennard-Jones potentials. In contrast, it is demonstrated that the Hansen–Verlet freezing rule is not valid for n-6 Lennard-Jones potentials.

ACKNOWLEDGMENTS

We thank the Australian Partnership for Advanced Computing (APAC) for a generous allocation of computing time. One of the authors (A.A.) thanks the Swinburne University of Technology for a postgraduate scholarship.

[1] P. A. Monson and D. A. Kofke, Adv. Chem. Phys. **115**, 113 (2000).
[2] D. Frenkel and J. P. McTague, Annu. Rev. Phys. Chem. **31**, 491 (1980).
[3] J. A. Barker and D. Henderson, J. Chem. Phys. **47**, 4714 (1967).
[4] J. D. Weeks, D. Chandler, and H. C. Andersen, J. Chem. Phys. **54**, 5237 (1971).
[5] H. C. Longuet-Higgins and B. Widom, Mol. Phys. **8**, 549 (1964).
[6] H. Meyer, O. Biermann, R. Faller, D. Reith, and F. Müller-Plathe, J. Chem. Phys. **113**, 6264 (2000).
[7] H. Okumura and F. Yonezawa, J. Chem. Phys. **113**, 9162 (2000).
[8] I. Charpentier and N. Jakse, J. Chem. Phys. **123**, 204910 (2005).
[9] K. Kiyohara, T. Spyriouni, K. E. Gubbins, and A. Z. Panagiotopoulos, Mol. Phys. **89**, 965 (1996).
[10] D. Heyes and J. Powles, Mol. Phys. **95**, 259 (1998).
[11] D. Heyes, G. Rickayzen, and A. Brańka, Mol. Phys. **102**, 2057 (2004).
[12] P. A. Gordon, J. Chem. Phys. **125**, 014504 (2006).
[13] J. Ge, G.-W. Wu, B. D. Todd, and R. J. Sadus, J. Chem. Phys. **119**, 11017 (2003).
[14] L. Wang and R. J. Sadus, Phys. Rev. E **74**, 031203 (2006).
[15] D. A. Kofke, J. Chem. Phys. **98**, 4149 (1993); R. Agrawal and D. A. Kofke, Mol. Phys. **85**, 43 (1995).
[16] J.-P. Hansen and L. Verlet, Phys. Rev. **184**, 151 (1969); J.-P. Hansen, Phys. Rev. A **2**, 221 (1970).
[17] W. B. Streett, H. J. Raveché, and R. D. Mountain, J. Chem. Phys. **61**, 1960 (1974); H. J. Raveché, R. D. Mountain, and W. B. Streett, *ibid.* **61**, 1970 (1974).
[18] A. J. C. Ladd and L. V. Woodcock, Chem. Phys. Lett. **51**, 155 (1977); Mol. Phys. **36**, 611 (1978).
[19] K. Chokappa and P. Clancy, Mol. Phys. **61**, 597 (1987); **61**, 617 (1987).
[20] T.-J. Hsu and C.-Y. Mou, Mol. Phys. **75**, 1329 (1992).
[21] A. Barroso and A. L. Ferreira, J. Chem. Phys. **116**, 7145 (2002).
[22] J. R. Morris and X. Song, J. Chem. Phys. **116**, 9352 (2002).
[23] J. R. Errington, J. Chem. Phys. **120**, 3130 (2004).
[24] E. A. Mastny and J. J. de Pablo, J. Chem. Phys. **122**, 124109 (2005); **127**, 104504 (2007).
[25] G. C. McNeil-Watson and N. B. Wilding, J. Chem. Phys. **124**, 064504 (2006).
[26] D. J. Evans and G. P. Morriss, *Statistical Mechanics of Nonequilibrium Liquids*, 2nd ed. (Academic, New York, 2008).
[27] R. J. Sadus, *Molecular Simulation of Fluids: Theory, Algorithms, and Object-Orientation* (Elsevier, Amsterdam, 1999).
[28] D. J. Evans, W. G. Hoover, B. H. Failor, B. Moran, and A. J. C. Ladd, Phys. Rev. A **28**, 1016 (1983).
[29] C. W. Gear, *Numerical Initial Value Problems in Ordinary Differential Equations* (Prentice-Hall, Englewood Cliffs, NJ, 1971).
[30] W. G. Hoover, M. Ross, K. W. Johnson, D. Henderson, J. A. Barker, and B. C. Brown, J. Chem. Phys. **52**, 4931 (1970).
[31] J. N. Cape and L. V. Woodcock, Chem. Phys. Lett. **59**, 271 (1978).
[32] R. Agrawal and D. A. Kofke, Phys. Rev. Lett. **74**, 122 (1995).
[33] D. C. Wang and A. P. Gast, J. Phys.: Condens. Matter **11**, 10133 (1999).
[34] S. Hess, M. Kröger, and H. Voigt, Physica A **250**, 58 (1998).
[35] W. G. Hoover, S. G. Gray, and K. W. Johnson, J. Chem. Phys. **55**, 1128 (1971).
[36] W. G. Hoover and F. H. Ree, J. Chem. Phys. **49**, 3609 (1968).
[37] W. T. Ashurst and W. G. Hoover, Phys. Rev. A **11**, 658 (1975).
[38] H. Matsuda and Y. Hiwatari, in *Cooperative Phenomena*, edited by H. Haken and M. Wagner (Springer, New York, 1973).
[39] M. A. van der Hoef, J. Chem. Phys. **113**, 8142 (2000).
[40] D. A. Kofke, in *Monte Carlo Methods in Chemistry*, Advances in Chemical Physics Vol. 105, edited by D. M. Ferguson, J. I. Siepmann, and D. G. Truhlar (Wiley, New York, 1999).
[41] P. J. Camp and G. N. Patey, J. Chem. Phys. **114**, 399 (2001); P. J. Camp, Phys. Rev. E **67**, 011503 (2003).
[42] Y. S. Wei and R. J. Sadus, AIChE J. **46**, 169 (2000).
[43] F. A. Lindemann, Phys. Z. **11**, 609 (1910).
[44] F. E. Simon and G. Z. Glatzel, Z. Anorg. Allg. Chem. **178**, 309 (1929).
[45] R. K. Crawford and W. B. Daniels, J. Chem. Phys. **55**, 565 (1971).
[46] M. Ross, Phys. Rev. **184**, 233 (1969).
[47] P. V. Giaquinta and G. Giunta, Physica A **187**, 145 (1992).
[48] S.-N. Luo, A. Strachan, and D. C. Swift, J. Chem. Phys. **122**, 194709 (2005).